Journal of Physics:
Conference Series

PAPER • **OPEN ACCESS**

Controllable Oil Adsorption from water Using Hydrophobic (Paraffin/Stearic Acid)/$CoFe_2O_4$ Magnetized Fibril Wax

To cite this article: M. M. Ghobashy 2024 *J. Phys.: Conf. Ser.* **2830** 012005

Journal of Physics: Conference Series **2830** (2024) 012005 doi:10.1088/1742-6596/2830/1/012005

Controllable Oil Adsorption from water Using Hydrophobic (Paraffin/Stearic Acid)/$CoFe_2O_4$ Magnetized Fibril Wax

M. M. Ghobashy*

*Radiation Research of Polymer Chemistry Department, National Centre for Radiation Research and Technology, Egyptian Atomic Energy Authority, Cairo, Egypt.

Mohamed_ghobashy@yahoo.com

Abstract. The development of efficient oil-water separation techniques is critical for mitigating environmental pollution from industrial oily wastewater. This study synthesized a hydrophobic and oleophilic (paraffin/stearic acid) (Par/St)/$CoFe_2O_4$ magnetized fibril wax for controllable adsorption and removal of waste engine oil from water. Structural and morphological characterization confirmed the successful incorporation of 30 wt% $CoFe_2O_4$ nanoparticles into the Par/St wax matrix with fibril morphology. Structural and morphological characterization using TEM, UV-Vis, FTIR, XRD, and SEM consistently confirmed the successful integration of $CoFe_2O_4$ nanoparticles into the Par/St wax matrix, forming fibrils with a high surface area. The oleophilic fibril demonstrated rapid adsorption and excellent removal efficiency of 99% for waste engine oil within 30 seconds. The fibrils could be magnetically guided for oil collection, ensuring reusable and eco-friendly oil remediation. This work introduces a novel solution for controllable oil spill clean-up and oily wastewater treatment.

1. Introduction

In recent years, developing specially designed sorbent materials has emerged as a promising approach for oil-water separation [1, 2]. These sorbents capitalize on certain materials' oleophilic and hydrophobic properties to selectively adsorb oils while repelling water [3]. Ideal sorbents for effective oil-water separation should possess high oil absorption capacities, selectivity, recyclability, and fast sorption kinetics [4]. Among various sorbent materials, organic-inorganic composite materials have attracted tremendous interest attributable to their tunable surface wettability, high porosity, and synergistic integration of unique components[5]. In particular, the fabrication of organic-inorganic composites with hydrophobic and superoleophilic characteristics has become an exciting route to engineer materials that can selectively absorb oils from water with great efficiency [6]. Hydrophobic surfaces containing micro/nanostructures along with low surface energy components can repel water while confining oil through their oleophilic nature [7]. This facilitates the selective absorption of oils and separation from water. Micro/nanomaterials like carbon-based materials, metal oxides, and polymers have been incorporated into hydrophobic organic materials to engineer oil-absorbing composites [8]. Among various nanomaterials, magnetic nanoparticles are highly advantageous for constructing oil sorbents since they impart magnetically guided oil recovery and recyclability to the composites [9]. This research aims to address the existing challenges by fabricating a novel (paraffin/stearic acid) (Par/St)/CoFe2O4 magnetically active fibril wax sorbent for controllable and recyclable oil-water separation. Paraffin wax

(Par) and stearic acid (St) are prospective candidates for constructing hydrophobic oil absorbents owing to their low cost [10], and chemical inertness properties [11]. Their tuning surface wettability also promotes selective oil absorption [12]. Incorporating magnetic $CoFe_2O_4$ nanoparticles into the Par/St wax to form magnetized fibrils can further impart magnetic responsiveness and recyclability [13]. $CoFe_2O_4$ possesses high magnetization and chemical stability, making it suitable for oil-water separation [14]. $CoFe_2O_4$ is a ferrimagnetic material with an inverse spinel structure. In this structure, the formula can be represented as $(Co^{2+})[Fe^{3+}]_2O_4$, where the parentheses indicate the tetrahedral sites (A sites) and the brackets indicate the octahedral sites (B sites). Unlike a normal spinel structure where divalent cations occupy the tetrahedral sites and trivalent cations occupy the octahedral sites, in an inverse spinel structure, the divalent Co^{2+} ions predominantly occupy the octahedral sites while Fe^{3+} ions are distributed between both tetrahedral and octahedral sites. Converting the composite into fibrils boosts the specific surface area and exposes more active sites for oil absorption [15]. The fibrillar morphology can mimic hydrophobic surfaces found in nature, facilitating excellent oil-water separation [16]. Magnetizing the fibrils enables their external control and recyclable application using simple magnets. This work is the first known report on fabricating (Par/St)/$CoFe_2O_4$ magnetized fibril wax for oil-water separation. It is hypothesized that the hydrophobic and superoleophilic wax-based fibrils with magnetic functionality can act as efficient absorbents for removing oils from water in a controllable and reusable manner. The first objective of this work is to synthesize oleophilic and hydrophobic Par/St wax incorporated with magnetic $CoFe_2O_4$ nanoparticles to construct the organic-inorganic composite material.

2. Experimental section

2.1. Materials

Cobalt nitrate hexahydrate [$Co(NO_3)_2.6H_2O$], iron (III) nitrate nonahydrate [Fe(NO3)3.9H2O], ammonium hydroxide (NH4OH), ethanol, paraffin wax, and stearic acid were supplied from Sigma Aldrich Co. and used as it is without further purification.

2.2. Synthesis of $CoFe_2O_4$

The synthesis of cobalt ferrite involved dissolving 14.58 g of cobalt nitrate hexahydrate [Co(NO3)2.6H2O] and 40.40 g of iron (III) nitrate nonahydrate [$Fe(NO_3)_3.9H_2O$] in a 100 mL volume of distilled water. The amounts of precursors were calculated to achieve a 1:2 molar ratio of Co: Fe, corresponding to the stoichiometric composition of $CoFe_2O_4$. This aqueous metal nitrate solution is stirred while adding a 4 M solution of ammonium hydroxide (NH_4OH) to achieve a pH of 10. The addition of NH4OH induces precipitation of cobalt and iron hydroxides which undergo further reaction to yield cobalt ferrite. The resulting precipitate is then washed repeatedly with ethanol (purity 98.0%) to remove any impurities. This purification wash process ensures that a high-purity cobalt ferrite product is obtained. The washed precipitate was dried at 80°C overnight. Finally, the dried precipitate was calcined in air at 800°C for 4 hours to obtain the desired CoFe2O4 nanoparticles.

2.3. Manufacture of the magnetized fibril wax consists of (Par/St)/$CoFe_2O_4$ nanocomposite

30 wt% of the previously synthesized cobalt ferrite ($CoFe_2O_4$) nanoparticles, corresponding to 3 g, were incorporated into a molten mixture of 7 g paraffin wax and 3 g stearic acid (Par/St) at 120°C under vigorous stirring. The ratio of paraffin wax to stearic acid was 7:3 by weight. This melt-mixing process allows homogeneous dispersion of the $CoFe_2O_4$ nanomaterial throughout the organic wax matrix. After achieving a uniform black-colored molten mixture, the (Par/St)/$CoFe_2O_4$ composite is converted into fibrous structures using an ultrasonication-based fibril procedure. This involves dropping the composite melt into a cold-water bath while simultaneously ultrasonicating it to induce solidification into micro-fibers. The result is fibril-shaped pellets of the (Par/St) wax infused with 30% $CoFe_2O_4$ that retains a high surface area morphology ideal for adsorption applications. This facile approach of melt-blending followed by ultrasonic produces magnetic wax-based organic-inorganic composite materials with versatile functionality. **Figure 1**, Cobalt Ferrite ($CoFe_2O_4$) exhibits an inverse spinel structure with a space group of $Fd^{-}3m$ [17]. In this structural arrangement, all tetrahedral A sites are fully occupied by Fe^{3+} cations, while the octahedral B sites demonstrate a random distribution of Co^{2+} and Fe^{3+} cations in

equal proportions. The inverse spinel structure is a characteristic feature of $CoFe_2O_4$, where the arrangement of metal cations within the crystal lattice follows a specific pattern. The occupancy of Fe^{3+} in the tetrahedral A sites and the equal distribution of Co^{2+} and Fe^{3+} in the octahedral B sites contribute to the unique crystallographic configuration of $CoFe_2O_4$, as inferred from the presented data in **Figure 1a**. The structure of paraffin wax and stearic acid is outlined in **Figures 1b** and **1c**, respectively.

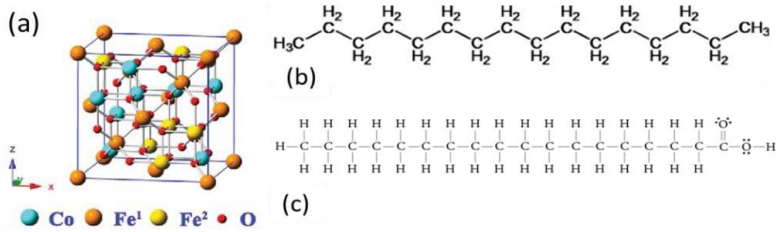

Figure 1. illustrates the crystal-chemical structures of Cobalt Ferrite ($CoFe_2O_4$) (a), paraffin wax (b), and Stearic acid (c)

2.4. Oil removal measurement

The oil removal measurement involved mixing 10 mL of automobile waste engine oil, obtained from a local automotive repair shop, with 90 mL of tap water. After allowing the mixture to settle, 1 g of the magnetized (Par/St)/$CoFe_2O_4$ wax composite was added and gently stirred for 30 seconds to facilitate oil adsorption onto the fibrils. The oil-adsorbed fibrils were then magnetically collected using an external neodymium magnet. The remaining aqueous solution was carefully transferred to a centrifuge tube and centrifuged at 3000 rpm for 10 minutes to separate any residual oil droplets. The volume of this separated oil layer was measured using a graduated volumetric tube and compared to the initial 10 mL of oil added to calculate the percentage removal efficiency. Triplicate experiments consistently showed an average oil removal efficiency of 98.8 ± 0.3% within the specified 30-second timeframe.

$$\text{Oil removal efficiency (\%)} = (W_o\text{-}W_r/W_o) * 100\text{--------} (1)$$

Where W_o is initial oil volume, W_r is residual oil volume

2.5. Characterization

Transmission electron microscopy (TEM) analysis was performed using a JEOL JEM-2100F field emission gun TEM operated at 200 kV. The TEM samples were prepared by drop-casting the $CoFe_2O_4$ nanoparticle suspension onto carbon-coated copper grids. X-ray diffraction (XRD) patterns were collected on a Rigaku Smart Lab X-ray diffractometer equipped with a Cu Kα radiation source (λ = 1.5406 Å) operated at 40 kV and 30 mA. The samples were scanned in the 2θ range of 10-80° with a step size of 0.02°. The morphology of the (Par/St)/$CoFe_2O_4$ magnetized fibril wax was examined using a Hitachi S-4800 field emission scanning electron microscope (FE-SEM) operated at an accelerating voltage of 5 kV. The samples were mounted on aluminum stubs using conductive carbon tape and sputter-coated with a thin layer of gold to minimize charging effects. Attenuated total reflectance Fourier transform infrared (ATR-FTIR) spectroscopy was performed on a Thermo Scientific Nicolet iS50 FTIR spectrometer equipped with a diamond ATR crystal. The spectra were collected in the range of 4000-400 cm^{-1} with a resolution of 4 cm^{-1} and averaged over 32 scans.

3. Results and discussion

3.1. The TEM analysis of $CoFe_2O_4$ nanoparticles

Figure 2 displays transmission electron microscopy (TEM) patterns of $CoFe_2O_4$, revealing well-defined particles with sizes ranging from 10 to 12 nm. The synthesized powders exhibit a uniform particle size distribution, crucial for material homogeneity. High-resolution TEM further identifies the crystallographic (311) plane with an interplanar distance of 0.24 nm, providing detailed insights into the atomic arrangement. The combined TEM and XRD analyses provide comprehensive insights into the morphological and structural characteristics of the synthesized $CoFe_2O_4$ nanoparticles. The TEM images reveal uniform particle size and morphology, while the XRD patterns validate the expected inverse

spinel crystal structure, ensuring the desired material properties for subsequent incorporation into the (Par/St)/$CoFe_2O_4$ composite.

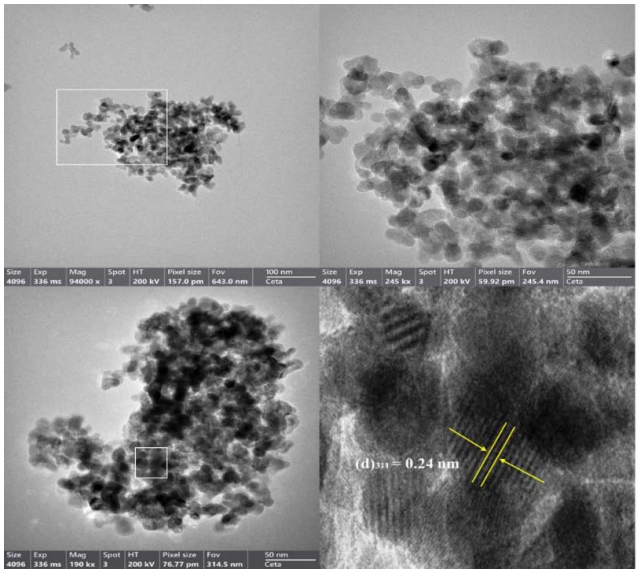

Figure 2. shows the TEM of $CoFe_2O_4$ nanoparticles (10-12 nm) with uniform distribution, highlighting the crystallographic (311) plane (0.24 nm).

3.2. The UV-Vis spectrophotometer of (Par/St)/$CoFe_2O_4$ nanocomposite

The peaks observed in **Figure 3** the UV-Vis spectrum of cobalt-ferrite at maximum wavelengths of 266 nm, 314 nm, and 355 nm can be attributed to electronic transitions within the material. The specific assignments of these peaks can vary depending on the crystal field splitting, ligand field effects, and other factors. The peak 266 nm could be associated with a transition involving the absorption of ultraviolet light by the cobalt ions in the cobalt-ferrite structure. It may be related to a charge transfer or d-d transition within the cobalt ions in the octahedral sites [18]. The peak at 314 nm could correspond to electronic transitions related to the Fe^{3+} ions in the octahedral sites, while the peak at 355 nm may be attributed to transitions involving the Fe^{3+} ions in the tetrahedral sites. The observed peaks confirm the expected electronic transitions within the $CoFe_2O_4$ nanoparticles, validating their inverse spinel structure and the fd-3m space group [19].

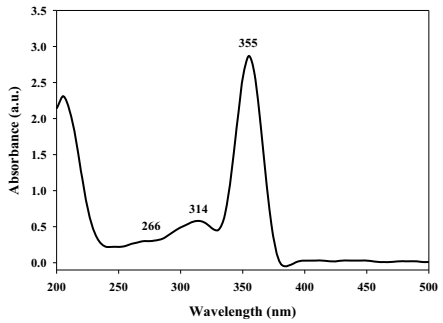

Figure 3. UV-Vis spectrum of cobalt-ferrite dispersed in (Par/St) matrix

3.3. The ATR/FTIR analysis of (Par/St)/$CoFe_2O_4$ nanocomposite

In the ATR-FT-IR spectra presented in **Figure 4a**, specific peaks for $CoFe_2O_4$ are observed at 3460 cm^{-1}, indicating O-H stretching vibrations, 1120 cm^{-1} attributed to the characteristic Fe-O bond stretching,

963 cm^{-1} corresponding to Co-O stretching, and 535 cm^{-1} associated with metal-oxygen vibrations. Moving to **Figure 4b**, which represents the FTIR spectra of (paraffin wax and stearic acid), the peaks at 3561 cm^{-1} are indicative of the O-H stretching in carboxylic acids, 2920 cm^{-1} and 2845 cm^{-1} represent C-H stretching in alkanes, 1705 cm^{-1} suggests C=O stretching in stearic acid, and 1112 cm^{-1} corresponds to C-O stretching. Finally, in **Figure 4c**, where the composite of (paraffin wax and stearic acid with $CoFe_2O_4$) is analyzed, the peaks at 3444 cm^{-1} denote O-H stretching in hydroxyl groups, 2912 cm^{-1} and 2845 cm^{-1} still represent C-H stretching in alkanes, 1697 cm^{-1} is associated with C=O stretching in esters, 1457 cm^{-1} indicates CH_2 bending, 1112 cm^{-1} corresponds to C-O stretching, and 722 cm^{-1} and 685 cm^{-1} suggest the presence of Co-O vibrations. Upon introducing $CoFe_2O_4$ in **Figure 4c**, noticeable shifts in peak positions, such as the O-H stretching at 3444 cm^{-1} and the C=O stretching at 1697 cm^{-1}, suggest potential interactions between the composite components. These shifts can be attributed to the formation of new chemical bonds, hydrogen bonding, or changes in the local environment around certain functional groups due to the incorporation of $CoFe_2O_4$.

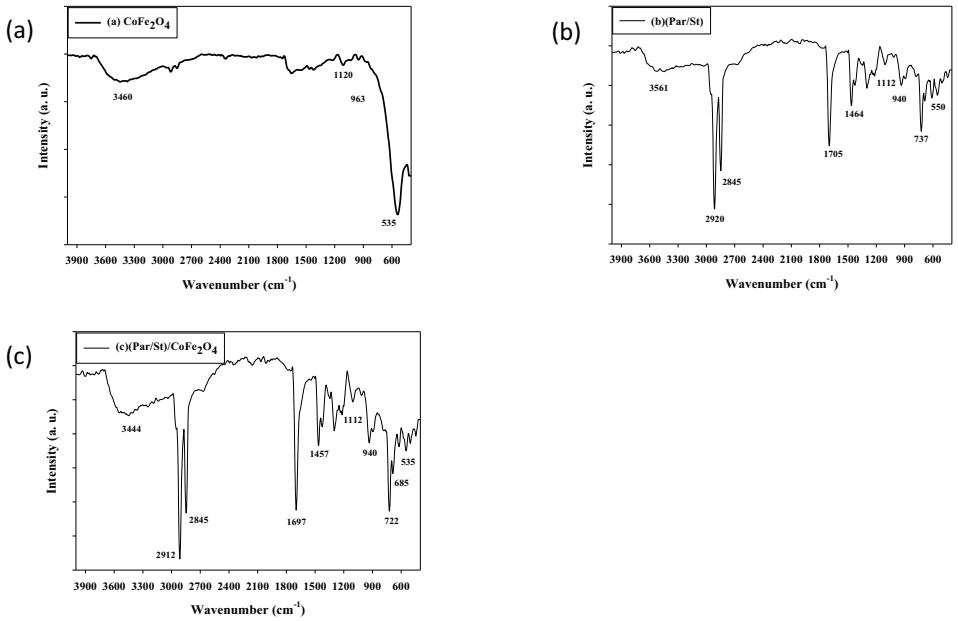

Figure 4. Attenuated Total Reflectance (ATR) T-IR spectra depicting the chemical composition of (a) $CoFe_2O_4$, (b) (paraffin wax and stearic acid), and (c) the composite material of (paraffin wax and stearic acid with $CoFe_2O_4$).

3.4. XRD analysis of (Par/St)/$CoFe_2O_4$ nanocomposite

The XRD peaks of $CoFe_2O_4$ in **Figure 5a** can be attributed to specific crystallographic planes based on the observed 2θ angles. The peak at 29.96° corresponds to the (220) plane, while the peak at 35.36° can be assigned to the (311) plane[14]. The peak at 42.84° is indicative of the (400) plane [20], and the peaks at 56.94° and 62.55° are associated with the (511) and (440) planes, respectively [21]. These assignments align with the characteristic diffraction pattern of a $CoFe_2O_4$ spinel structure. The distinct peaks and their corresponding crystallographic planes provide an inverse spinel crystal structure. The XRD peaks of the paraffin wax and stearic acid blend in **Figure 5b** are indicative of specific crystallographic planes, as determined by the observed 2θ angles. The peak at 20.65° can be attributed to the (020) plane, while the peak at 21.54° corresponds to the (110) plane. The peak at 22.93° is indicative of the (021) plane, and the peak at 39.79° is associated with the (200) plane [22]. These assignments follow the characteristic diffraction pattern expected for the crystalline structure of the paraffin wax and stearic acid composite. The distinct peaks and their corresponding crystallographic planes provide valuable information about the arrangement and packing of molecules within the crystalline lattice, contributing to a comprehensive understanding of the material's structural properties. The XRD peaks of the paraffin

wax and stearic acid blend, along with CoFe2O4, reveal distinct patterns corresponding to specific crystallographic planes in **Figure 5c**. In the case of the paraffin wax and stearic acid blend, the peaks at 20.58°, 21.40°, and 22.84° are associated with the (020), (110), and (021) planes, respectively. For $CoFe_2O_4$, the peaks at 28.90°, 34.94°, 35.16°, 39.62°, 42.78°, 56.13°, and 61.77° are attributed to the (220), (311), (222), (400), (331), (511), and (440) planes, respectively [23]. These assignments align with the expected diffraction angles for the respective crystal structures. The slight shifts observed in the peak positions for both the paraffin wax/stearic acid and $CoFe_2O_4$ components in the composite material (**Figure 5c**) compared to their patterns (**Figures 5a** and **5b**) suggest potential interactions, such as chemical bonding or hydrogen bonding, between the $CoFe_2O_4$ nanoparticles and the organic matrix. The XRD analysis, in combination with other characterization techniques like TEM and UV-Vis spectroscopy, provides strong evidence for the formation of the inverse spinel $CoFe_2O_4$ nanoparticles and their successful incorporation into the (Par/St)/$CoFe_2O_4$ composite material.

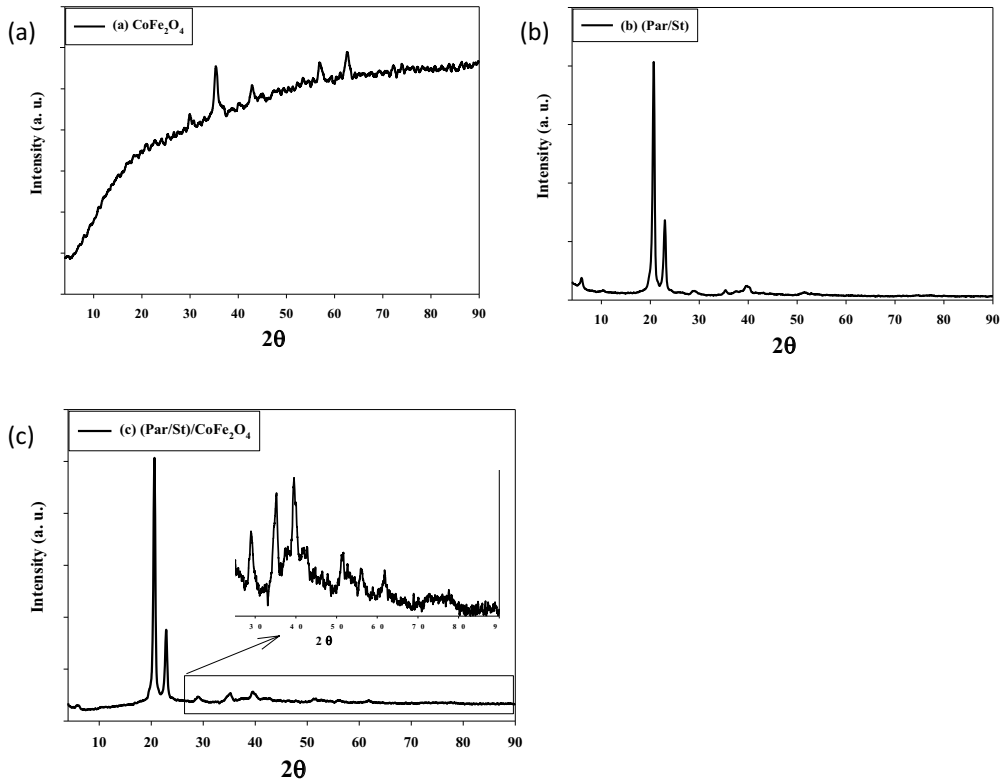

Figure 5. the XRD chart depicting the crystal composition of (a) $CoFe_2O_4$, (b) (paraffin wax and stearic acid), and (c) the composite material of (paraffin wax and stearic acid with $CoFe_2O_4$).

3.5. The SEM and contact angle analysis of (Par/St)/$CoFe_2O_4$ magnetized fibril wax

The SEM image in **Figure 6a** of (Par/St)/$CoFe_2O_4$ reveals a distinctive fibril form, showcasing the unique morphology of the material. The elongated, thread-like structures, characteristic of fibrils, suggest a specific arrangement or assembly of (Par/St)/CoFe2O4 components. This intricate morphology can significantly influence the material's properties and applications in oil removal. **Figure 6b** shows The contact angle (θ) of 96.67° exhibited by the (Par/St)/CoFe2O4 magnetized fibril wax indicates a hydrophobic surface, a property that is crucial for its effective oil absorption and repulsion of water.

Figure 6. The SEM image of (Par/St)/$CoFe_2O_4$ magnetized fibril wax (a) and (b) contact angle with (θ = 96.67°) The left picture shows the microscope picture of (Par/St)/$CoFe_2O_4$ magnetized fibril wax .

3.6. Selective oil adsorption

The removal of waste engine oils is a critical endeavor that holds significant environmental benefits. Engine oils, as they undergo service, accumulate various contaminants, including carbon residue, gums, metals, varnish, ash, water, and asphaltic compounds. While the molecular structure of lubricant oils remains largely intact during use, the increasing concentration of contaminants poses a threat to the environment. When released, these oils liberate detrimental metals and other pollutants, contributing to environmental degradation. Addressing this challenge, a novel approach has been explored, leveraging the unique properties of hydrophobic (Par/St)$CoFe_2O_4$ magnetized fibril wax. This innovative material exhibits hydrophobic and oleophilic characteristics, making it particularly suitable for applications in remote-controlled oil–water separation. The oleophilic nature of the wax ensures a strong affinity for oil, facilitating effective adsorption and separation from water. In the conducted study, the magnetically controllable oil adsorption capacity of (Par/St)$CoFe_2O_4$ was put to the test. **Figure 7** illustrates a microfibril of the magnetized wax in a petri dish containing a mixture of waste engine oil and water. This specific oil originates from automobile engines, characterized by high levels of carbon, ashes, and various compounds. The experiment demonstrates the remarkable efficiency of the magnetic fibril wax in adsorbing oil from the mixed solution. The process is elegantly simple. Introducing the magnetic fibril wax into the oil-water mixture lets the pellets float on the surface, come into contact with the oil, and rapidly adsorb from the solution. Notably, the controllability of the oil removal process is a key feature. External magnets can be employed to guide the magnetic pellets wax toward collection points, allowing for efficient and reusable oil removal. **Figure 7a** showcases the oleophilic behavior of the fibril, depicting how the magnetic pellet wax adsorbs a substantial amount of oil, reaching an impressive 99% removal within just 30 seconds. This high efficiency in oil removal and the controllable nature of

the process present a promising solution for managing and mitigating the environmental impact of waste engine oils. **Figure 7b** shows the sensitive (Par/St)$CoFe_2O_4$ magnetized fibril wax removed by an external magnet without loss of waste oil. Demonstrates the ability to be completely removed from the contaminated area using an external magnet without any loss or leakage of the absorbed oil.

Figure 7 illustrates the efficient and controllable oil adsorption capabilities of (Par/St)$CoFe_2O_4$ magnetized fibril wax in a waste engine oil-water mixture.

4. Conclusion

This study successfully developed a novel hydrophobic and oleophilic (Par/St)/$CoFe_2O_4$ magnetized fibril wax composite material for efficient and controllable oil-water separation. The strategic integration of magnetic CoFe2O4 nanoparticles into the paraffin/stearic acid wax matrix, coupled with the fibrillar morphology, endowed the material with unique properties tailored for oil remediation applications. Comprehensive characterization techniques, including TEM, UV-Vis spectroscopy, FTIR, XRD, and SEM, consistently validated the successful synthesis and confirmed the incorporation of $CoFe_2O_4$ nanoparticles within the fibrillar wax composite. The slight shifts observed in the XRD peaks suggested potential chemical or hydrogen bonding interactions between the nanoparticles and the organic matrix, contributing to the material's stability and performance. Significantly, the (Par/St)/$CoFe_2O_4$ magnetized fibril wax demonstrated remarkable oil removal efficiency, achieving an impressive 99% separation of waste engine oil from water within just 30 seconds. This outstanding performance can be attributed to the synergistic effects of the hydrophobic and oleophilic nature of the wax matrix, the high surface area provided by the fibrillar morphology, and the magnetic responsiveness imparted by the $CoFe_2O_4$ nanoparticles. The magnetic controllability of the fibrils enabled efficient oil collection and removal through external magnetic guidance, eliminating the need for complex separation processes. This feature, combined with the material's reusability, presents a sustainable and cost-effective solution for various oil remediation applications, including industrial oily wastewater treatment and oil spill clean-up.

References

[1] Gayed H M and Ghobashy M M 2024 Fabrication of jelly like material from rLLDPE by a binary approach based on gamma irradiation and thermal processing for oil remediation Discover Applied Sciences 6 1-17
[2] Gayed H M and Ghobashy M M 2023 Gamma irradiation-enhanced performance of waste LLDPE thermally transformed into advanced sponge-like material for oil decontamination Scientific Reports 13 19222
[3] Mubarak M F, Selim H, Hawash H B and Hemdan M 2024 Flexible, durable, and anti-fouling maghemite copper oxide nanocomposite-based membrane with ultra-high flux and efficiency for oil-in-water emulsions separation Environmental Science and Pollution Research 31 2297-313

[4] Sankaranarayanan S, Lakshmi D S, Vivekanandhan S and Ngamcharussrivichai C 2021 Biocarbons as emerging and sustainable hydrophobic/oleophilic sorbent materials for oil/water separation Sustainable Materials and Technologies 28 e00268
[5] Rahmanian V, Pirzada T, Wang S and Khan S A 2021 Cellulose-Based Hybrid Aerogels: Strategies toward Design and Functionality Advanced Materials 33 2102892
[6] Abu-Thabit N Y, Uwaezuoke O J and Elella M H A 2022 Hydrophobic nanohybrid sponges for separation of oil/water mixtures Chemosphere 294 133644
[7] Ghaffari S, Aliofkhazraei M, Darband G B, Zakeri A and Ahmadi E 2019 Review of superoleophobic surfaces: Evaluation, fabrication methods, and industrial applications Surfaces and Interfaces 17 100340
[8] Hoang A T, Nižetić S, Duong X Q, Rowinski L and Nguyen X P 2021 Advanced super-hydrophobic polymer-based porous absorbents for the treatment of oil-polluted water Chemosphere 277 130274
[9] Singh B, Kumar S, Kishore B and Narayanan T N 2020 Magnetic scaffolds in oil spill applications Environmental Science: Water Research & Technology 6 436-63
[10] Bazaka K, Jacob M V and Ostrikov K 2016 Sustainable life cycles of natural-precursor-derived nanocarbons Chemical reviews 116 163-214
[11] Romero S, Minari R J and Collins S E 2021 Bio-paraffin from Soybean Oil as Eco-friendly Alternative to Mineral Waxes Industrial & Engineering Chemistry Research 60 5364-73
[12] Bayer I S, Martiradonna L and Athanassiou A 2013 Nanostructured Lubricated Silver Flake/Polymer Composites Exhibiting Robust Hydrophobicity Advances in Contact Angle, Wettability and Adhesion 1 203-25
[13] Abdel Maksoud M I A, Ghobashy M M, Kodous A S, Fahim R A, Osman A I, Al-Muhtaseb A a H, Rooney D W, Mamdouh M A, Nady N and Ashour A H 2022 Insights on magnetic spinel ferrites for targeted drug delivery and hyperthermia applications Nanotechnology Reviews 11 372-413
[14] Gan W, Gao L, Zhang W, Li J, Cai L and Zhan X 2016 Removal of oils from water surface via useful recyclable CoFe2O4/sawdust composites under magnetic field Materials & Design 98 194-200
[15] Liu R, Hou L, Yue G, Li H, Zhang J, Liu J, Miao B, Wang N, Bai J and Cui Z 2022 Progress of fabrication and applications of electrospun hierarchically porous nanofibers Advanced Fiber Materials 4 604-30
[16] Chai J, Wang G, Zhang A, Zhao G and Park C B 2024 Hydrophobic nanofibrous polytetrafluoroethylene and composite membranes with tunable adhesion for micro-droplet manipulation, self-cleaning and oil/water separation Journal of Environmental Chemical Engineering 12 112355
[17] Zeng X, Zhang J, Zhu S, Deng X, Ma H, Zhang J, Zhang Q, Li P, Xue D and Mellors N J 2017 Direct observation of cation distributions of ideal inverse spinel CoFe 2 O 4 nanofibres and correlated magnetic properties Nanoscale 9 7493-500
[18] Jebali S, Meftah M, Mejri C, Ben Haj Amara A and Oueslati W 2023 Enhancement of Photocatalytic Activity and Microstructural Growth of Cobalt-Substituted Ba1− xCoxTiO3 {x= 0,…, 1} Heterostructure ChemEngineering 7 43
[19] Al Sdran N, Shkir M, Ali H E and Chandekar K V 2024 Enhanced structural, optical, dielectric, and electrical properties of CoFe2O4 nanostructures: Effect of variation of citric acid concentration Ceramics International 50 4673-86
[20] Al-Musawi T J, Mengelizadeh N, Kassim W M S, Sillanpää M, Siddiqui S H, Shahbaksh S and Balarak D 2022 Sonophotocatalytic degradation and operational parameters optimization of diazinon using magnetic cobalt–graphene nanocomposite as a catalyst Journal of Water Process Engineering 46 102548
[21] Zhao S and Ma D 2010 Preparation of CoFe2O4 nanocrystallites by solvothermal process and its catalytic activity on the thermal decomposition of ammonium perchlorate Journal of Nanomaterials 2010 1-5
[22] Luyt A S and Krupa I 2008 Thermal behaviour of low and high molecular weight paraffin waxes used for designing phase change materials Thermochimica Acta 467 117-20

[23] Loh K-S, Lee Y H, Musa A, Salmah A A and Zamri I 2008 Use of Fe3O4 nanoparticles for enhancement of biosensor response to the herbicide 2, 4-dichlorophenoxyacetic acid Sensors 8 5775-91